IOP PUBLISHING JOURNAL OF PHYSICS: CONDENSED MATTER

J. Phys.: Condens. Matter **19** (2007) 000000 (10pp) UNCORRECTED PROOF

Flexible tissue with fibres interacting with an adhesive surface

A E Filippov[1] **and V Popov**[2,3]

[1] Donetsk Institute for Physics and Engineering of NASU, 83144, Donetsk, Ukraine
[2] Technische Universität Berlin, Institut für Mechanik, D-10623 Berlin, Germany

E-mail: v.popov@tu-berlin.de

Received 23 October 2006, in final form 22 December 2006
Published
Online at stacks.iop.org/JPhysCM/19/000000

Abstract

An artificial structure of a flexible tissue with rotatable elastic fibres that interact with a rough fractal surface is simulated numerically. We concentrate on a realistic system of relatively hard but slightly flexible fibres contacting an adhesive surface. It is shown that if the flexibility in the direction orthogonal to the average surface is limited the additional degrees of freedom in other directions become important for better adaptation of the stiff fibres to the fractal surface. Attachment and detachment scenarios with different starting distances, surface roughnesses and pulling angles are simulated.

1. Introduction

The existence of a powerful natural system (the gecko's foot) that applies dry adhesion at nanoscales has stimulated great theoretical and experimental activity during last few years [1–10]. It has also encouraged practical efforts in nanotechnology to fabricate surface patterns with polymers to mimic the structure of setae and spatulas in gecko foot-hair [6–10]. The problem is challenging because the natural foot of the gecko has a very complex structure and its adhesion is a combined effect of many impacts on different scales [4, 11–14]. The foot is covered by a layer of hair (fibres). Each of these fibres branches out into about 10^3 thinner ones. These smaller fibres end with a thin (5–10 nm) leaf-like plate. The finest structure is already small enough to be able to follow the surface roughness profile at almost molecular scale. The foot is a result of development driven by the principle of natural selection and it is supposed normally to be highly optimized. In its turn, being a result of natural selection, it certainly conserves incidental fingerprints of some fossil animal which gradually evolved into the present-day creature. It is not necessary to copy the natural system absolutely, but just use the main idea of fibres to make artificial molecular structures (like nanotubes) as technological and as efficiently as possible. Some of these synthetic systems already have

[3] Author to whom any correspondence should be addressed.

0953-8984/07/000000+10$30.00

Ascii/Word
JPC/cm235571/PAP
Printed 8/2/2007

Focal Image
(*Ed: Bridget*)

CRC data

File name First page
Date req. Last page
Issue no. Total pages
Artnum Cover date

properties comparable to natural ones. The artificial structures are based on relatively hard materials like carbon nanotubes or micro-electromechanically produced 'organorods' [9, 10] and show very good adhesive properties.

In our previous paper [15] we simulated numerically the artificial structure of elastic fibres contacting with a rough fractal surface by van der Waals forces. The main goal was to find an optimal relation between the system parameters. The force balance equations were solved for different values of the elastic constant and variable surface roughness. An optimal elasticity has been calculated to provide the maximum cohesive force between the plate and the surface. In agreement with experimental observations [9, 10], it was found that high flexibility of the fibres is not always good for the efficiency of the system and artificial adhesives must be made from sufficiently stiff polymers.

Novel nanostructures have a common theoretical advantage: it is easier to simulate them numerically than complex mesoscopic ones. But even an artificial nano-brush is still a many-body system moving in all three dimensions. To simplify the model in [15] we restricted the motion to the z-direction (which is orthogonal to the mean positions of two contacting plates) only. The effective elasticity of the fibres K_{eff} in this case was treated as a combination of bending of the hairs with their extension under van der Waals force. The model structure is quite simple but still recalls recently fabricated polymer surfaces with multi-walled carbon hairs [10]. These structures form dense nanoscale brushes of almost parallel bundles providing extremely good contact to a surface on the nanoscale. They have a strong nanometre-level adhesion force/area relation of $1.6 \pm 0.5 \times 10^{-2}$ nN nm^{-2} that is 200 times higher than that observed for gecko foot-hairs. Typical stress–displacement curves during a step loading–unloading cycle show a high hysteresis loop with an adhesion region up to 20 nm.

From theoretical point of view these structures differ from the natural hair system. In the natural system the finest hair does not reach the molecular scale and ends in a thin spatula. As a result, the model can use a simple pull-off contact force, but must account for adjustment of the spatula to the rough surface [11]. The properties of the artificial system are determined by a combination of van der Waals forces and energy dissipation during the elongation of the carbon nanotubes which comes from their material properties [10]. The van der Waals forces originate from extremely large contact areas with a single nanotube, while the energy dissipation is due to their exceptionally high strength and extraordinary flexibility under large strains.

Despite its efficiency for the numerical simulations, the model [15] allowing only motions in the z-direction requires further development. Besides theoretical understanding of this there are recent experimental observations which favour a strong importance of orthogonal motion in the system under consideration. In particular, sliding or vibrating in the orthogonal direction of the plate which is transferred down to molecular scales may increase the contact area and change the relation between the adhesion and friction impacts to an interaction between the surfaces depending on the contact roughness or angle of the force applied [11, 13, 14].

Below we extend the model to incorporate an additional degree of freedom to allow bending and rotation of the fibres. We study how the intensity of the interaction as well as attachment and detachment scenarios depend on different starting distances, surface roughnesses and pulling angles.

2. Model and simulations

For the reasons given above the artificial system has to combine two features: soft tissues on relatively high scales to preliminarily adapt the large-scale part of the surface structure, and hard short fibres to fit the very last micro- and nanoscales. To deal with this problem we construct an advanced model which includes the following elements:

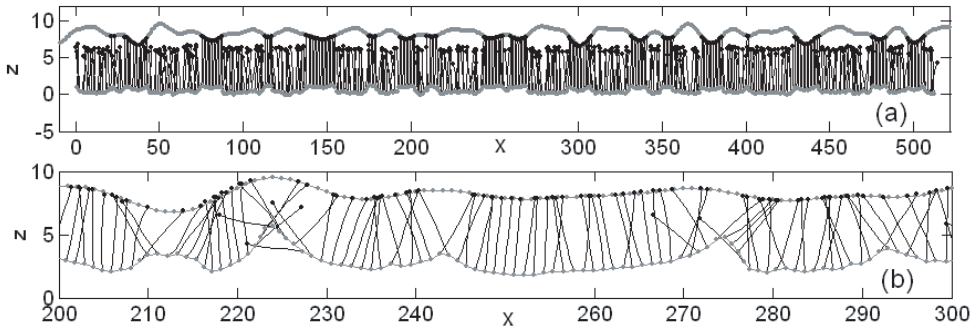

Figure 1. Conceptual structure of the model. Bold grey upper and lower lines represent the fragments of the rough surface and flexible tissue, respectively. The lines with black circles show the instantaneous positions of the elastic fibres. Subplot (a) presents an early stage of the contact with many disconnected bonds. A closer view of the system at later stage, when the majority of the fibres have distorted to attach to the surface is shown in subplot (b).

(1) flexible soft tissue which is organized as a 'molecular chain' in the x-direction.
(2) Relatively hard fibres attached to the tissue. The stiffness of the fibres is much higher than it is in the chain but they are still flexible.
(3) An adhesive surface which attracts the ends of the fibres by the van der Waals potential. The surface has a semi-fractal structure with a given Fourier spectrum and amplitude of roughness.
(4) Random noise simulating both dynamic chaos caused by the macroscopic motion transferred down to the nanoscale and temperature fluctuations accompanied by the dissipation.
(5) An external force that can be applied to any part of the tissue at an arbitrary angle.

The conceptual structure of the model is illustrated in figure 1. The adhesive hard surface is shown by the upper bold line, flexible 'foot' tissue is represented by the lower grey line. The fibres are thin black lines attached to this tissue. In equilibrium each fibre forms some angle with the tissue. Van der Waals attraction to the surface as well as repulsion from the bulk bends the fibres. In the general case, the fibres find a compromise position. The upper subplot in figure 1(a) shows the early state of the system, when a relatively large distance between the foot and the tissue is kept fixed at the beginning. At this stage there are many fibres remote from the surface. These fibres cannot attach to the surface at the moment. The later stage of the attraction is shown in the second subplot figure 1(b), where a relatively short part of the system is shown to make visible the fibres, which are bent and/or extended and attached to different points of the upper surface.

The model equations are basically close to the equations used in [15]. The potential that connects each fibre with the surface is the van der Waals potential:

$$U_{\mathrm{VdW}} = U\left[\left(\frac{r}{r_{\mathrm{VdW}}}\right)^{12} - 2\left(\frac{r}{r_{\mathrm{VdW}}}\right)^{-6}\right]\Big/ 12. \tag{1}$$

Here U is a characteristic energy of the adhesion potential, $r = \{x, z\}$ is a two-dimensional vector and r_{VdW} is a position of the potential minimum. The fibres should be constructed from a number of segments $j = 1, 2, \ldots, n_{\max}$ with coordinates $\{r_i, r_j\}$. It is supposed that only the final segment of every fibre can be attached to the surface via the van der Waals potential.

This means that the term $U_{\rm VdW} = U_{\rm vdW}^{n_{\max}}$ in energy exists for the $j = n_{\max}$ only. Each flexible segment can be elastically extended with an elastic energy

$$U_{\rm elastic}^{ij} = K_{\rm eff}(r_i - r_j)^2/2. \tag{2}$$

Besides, there is a bending energy which prevents two strong deviations of the direction in every pair of nearest segments:

$$U_{\rm bending}^{j} = K_{\rm bending}[1 - (r_j - r_{j+1}) \cdot (r_{j-1} - r_j)/|(r_j - r_{j+1})| \cdot |(r_{j-1} - r_j)|]. \tag{3}$$

As usual, corresponding forces in the equations are equal to the derivatives: $F_{\rm VdW}^{z} = \partial U_{\rm VdW}/\partial z$; $F_{\rm VdW}^{x} = \partial U_{\rm VdW}/\partial x$, $F_{\rm elastic}^{z,ij} = \partial U_{\rm elastic}^{ij}/\partial z$; $F_{\rm elastic}^{x,ij} = \partial U_{\rm elastic}^{ij}/\partial x$ and $F_{\rm bending}^{z,j} = \partial U_{\rm bending}^{j}/\partial z$; $F_{\rm bending}^{x,j} = \partial U_{\rm bending}^{j}/\partial x$, respectively. In the zero approximation, one can neglect any interaction between the bonds.

Below it is convenient to normalize all the energies, noise intensity and space scales to the units of the van der Waals potential $F_{\rm VdW}$ and $\zeta_{\rm VdW}$. Typical magnitudes for the values are as follows: $F_{\rm VdW} = 10$–70 nN, $\sigma = 0.1$–1.0 nm (in particular, for nanotubes $\sigma = 0.34$ nm and $\varepsilon = 12$ meV). The elastic constant in the units $K = K_{\rm eff}\sigma^2$ belongs to the interval $0.1 < K < 10$, stiffness $S = 0.1$ K.

In these units one has

$$\begin{aligned} &U_{\rm VdW} = U\left[r^{12} - 2r^{-6}\right]/12; \qquad U_{\rm elastic}^{ij} = K(r_i - r_j)^2/2; \\ &U_{\rm bending}^{j} = S[1 - (r_j - r_{j+1}) \cdot (r_{j-1} - r_j)/|(r_j - r_{j+1})| \cdot |(r_{j-1} - r_j)|]. \end{aligned} \tag{4}$$

The randomness in the system is caused by the fractal surface $z = w(x)$, fibre dynamics and temperature fluctuations which are important at molecular scales. In a numerical model a fractal surface can be generated as a data array according to the standard definition:

$$w(x) = \frac{1}{2\pi}\int_{q_{\min}}^{q_{\max}} c(q)\cos(qx + \xi), \tag{5}$$

where $c(q) = c_0 q^{\alpha}$ and $\zeta(x)$ is a random δ-correlated phase:

$$\langle \zeta(x)\zeta(x')\rangle = \delta(x - x'). \tag{6}$$

The actual surface $w(x)$ is semi-fractal, it has some limited spectrum of wavevectors $q_{\min} < q < q_{\max}$ and its standard deviation is limited too

$$\langle (w(x) - \langle w(x)\rangle)^2\rangle^{1/2} \simeq A. \tag{7}$$

Here factor A describes a characteristic physical 'roughness' of the surface. For some regions of the parameters the total potential has two valleys of comparable depth. At fluctuating parameters these comparable energy valleys provoke dynamic jumps of the ending fibre segments between two alternative (attached–detached) states. The time averaged dynamic exchange leads to an attraction of the tissue to the surface [15]. Below in numerical experiments we measure all distances in units of fixed interval between two nearest fibres $\Delta x_k = \text{const} \equiv 1$ nm and vary the roughness amplitude up to $A_{\max} = 10\Delta x_k$. In the same units the elastic constant is kept fixed at $K = 1$ and the stiffness is changed up to $S_{\max} = 10$ K.

The last addition which completes the equation of motion relates to the flexible tissue. We suppose that last segment of each fibre is rigidly attached to the tissue. This means that the coordinates of the tissue segments coincide with the positions of the first elements of the fibres: $\{x_k^{j=1}, z_k^{j=1}\}$. It is supposed that model tissue has its own elasticity K_1^z in the z-direction $U_{\rm elastic}^{1} = K_1^z[(z_k^1 - z_{k+1}^1)^2 + (z_k^1 - z_{k-1}^1)^2]/2$ while the distance between the segments in the x-direction (defining an array of the fibres) is kept fixed at $\Delta x_k = \text{const} \equiv 1$. The tissue is also

kept in the z-direction by an external force F^z_{external}. As result, one has additional interactions for the coordinates $\{z_k^{j=1}\}$:

$$F^{z,1}_{\text{elastic}} = \partial U^1_{\text{elastic}}/\partial z; \qquad \text{and} \qquad F^{z,1}_k = F^z_{\text{external}}. \tag{8}$$

The complete set of dynamic equations can now be written as follows:

$$\begin{aligned}
\frac{\partial^2 z_k^j}{\partial t^2} &= -\gamma \frac{\partial z_k^j}{\partial t} + F^{z,ji}_{\text{elastic},k} + F^{z,j}_{\text{bending},k} + F^{z,j=n_{\max}}_{\text{VdW},k} + \delta_{j1}(F^{z,1}_{\text{elastic},k} + F^z_{\text{external}}) + \zeta(x_k^j, z_k^j; t);\\
\frac{\partial^2 x_k^j}{\partial t^2} &= -\gamma \frac{\partial x_k^j}{\partial t} + F^{x,ji}_{\text{elastic},k} + F^{x,j}_{\text{bending},k} + F^{x,j=n_{\max}}_{\text{VdW},k} + \zeta(x_k^j, z_k^j; t).
\end{aligned} \tag{9}$$

Here δ_{j1} is a Kronecker symbol. The random source $\zeta(z_j; t)$ and dissipation $\gamma \partial z_j/\partial t$ are also included to simulate both thermal and dynamic impacts to the system with an effective temperature T_{eff}:

$$\langle \zeta(x_k^j, z_k^j; t)\zeta(x_{k'}^{j'}, z_{k'}^{j'}; t')\rangle = D\delta(x_{k'}^{j'} - x_k^j)\delta(z_{k'}^{j'} - z_k^j)\delta(t' - t); \qquad D = 2k_{\text{B}}\gamma T_{\text{eff}}. \tag{10}$$

Random noise here simulates both temperature fluctuations and dynamic chaos transferred to the nanoscale from macroscopic motions of the system. It works jointly with the dissipation to maintain an average thermodynamic equilibrium. The dissipation describes an exchange with all other degrees of freedom which are not included in the model. These two impacts do not significantly influence the scenarios while the energy of the noise is much smaller than the other energies of the problem. However, it is important to keep 'temperature' in the equations to control the global stability of the solutions, to randomize initial conditions and to accumulate statistics over realizations when necessary. For example, one can check that weak fluctuations even support the attachment process, but strong fluctuations destroy the contact as expected.

We have performed a set of numerical experiments with the above system. The typical procedure is organized as follows. We generate a fragment of random rough surface (new each time) and place a flexible tissue at some initial distance z_0. Initially it is flat with fibres arranged as a regular array of lines and oriented orthogonally to the tissue in the direction of the surface. After this, the system is allowed to move naturally according to the equations (8)–(10) up to a dynamic equilibrium. The time run to get to equilibrium is determined by a characteristic relaxation rate $t_{\max} \propto \gamma^{-1}$. The coefficient here can be estimated from the time behaviour in real simulations and normally the run takes approximately $t_{\max} \cong 200\gamma^{-1}$.

In a real system the density of the fibres is relatively high and there is an interaction between them. This interaction has been ignored in the present simulations for the standard reasons of numerical work: it transforms the model into a many-body problem, which is very time-consuming. Besides, the complexity of the many-body problem often masks the main features of the problem under the interplay of many parameters and makes it difficult to extract important information. An overlap of the fibres is ignored too in the 2D (1 + 1 dimensional) problem. Their formal intersection in x–z space is treated as a projection from real 3D space.

Our observation shows that at the intermediate stage of the process the ends of the revolving flexible fibres move intensively along the surface in the x-direction. This ability to move along the x-axis allows the fibres to adapt much better to a fractal surface than was possible for a hard 'bristle' (with the fibres extendable in the z-direction only) [15]. As a result, transverse motion leads to a strongly nonuniform redistribution of the contact density along the surface. To some extent, one can say that fractal *redistribution of the fibres along the transverse direction compensates for fractal surface structure in the z-direction*. Figure 2 illustrates a typical redistribution of the fibres at intermediate time moments of their adaptation to the surface. The instantaneous positions of good fibre attachment are seen in subplot (a).

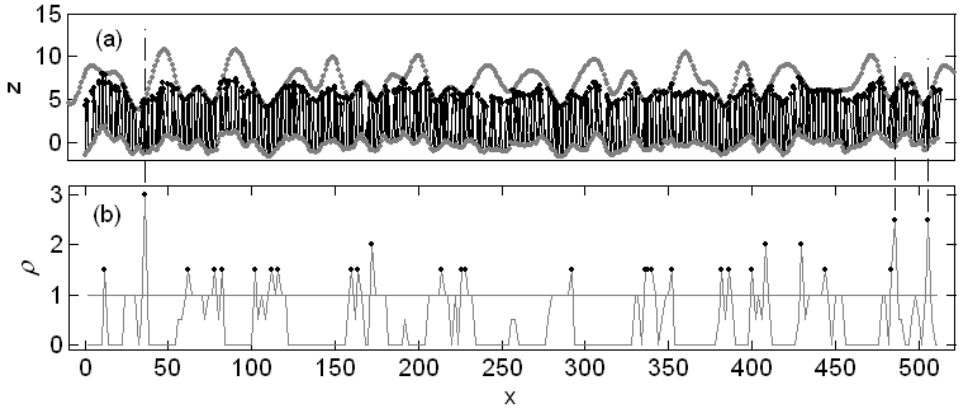

Figure 2. Comparison between the instant places of good fibre attachment (a) and nonuniform density distribution (b) of the attachment positions along the x-axis (normalized to the mean density). The places with the highest densities are marked by the dash–dot lines.

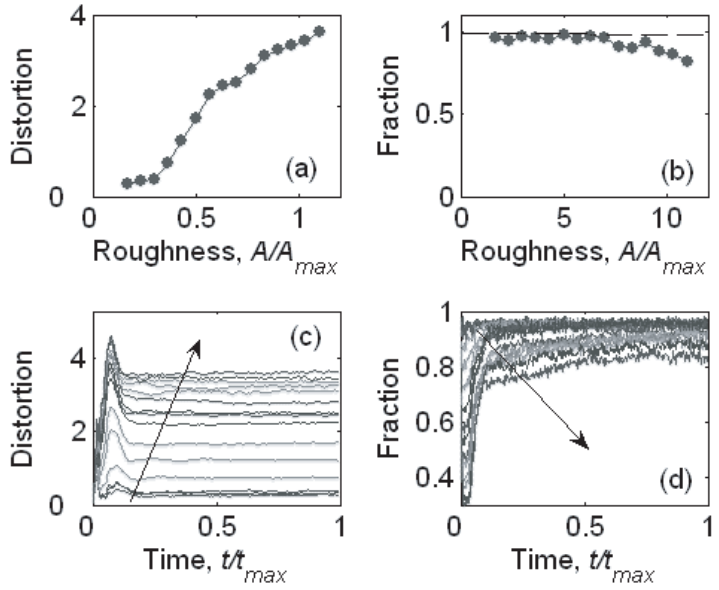

Figure 3. Mean distortion of the fibres (a) and fraction of the attached bonds (b) as functions of the surface roughness. The subplots (c) and (d), respectively, illustrate the numerical procedure. For each roughness the system starts from a trial state with completely disconnected bonds and tends to a dynamic equilibrium. We average desirable variables over an ensemble of the fibres and calculate the time dependences of the mean values. Then we omit an initial transient period and overage them over the second half of the time-run.

They are compared to a nonuniform density distribution of the attachment positions along the x-axis in subplot (b). The density is normalized to a mean fibre density over the system equal to $\rho_0 = N_{\text{fibres}}/L_{\text{tissue}}$. The places with the highest densities are marked by dash–dot lines.

The mechanical properties of the system depend on the parameters surface roughness, fibre stiffness and elasticity. We performed the above numerical experiments for wide intervals of the parameters. The results are summarized in figures 3–5. For each parameter the system starts

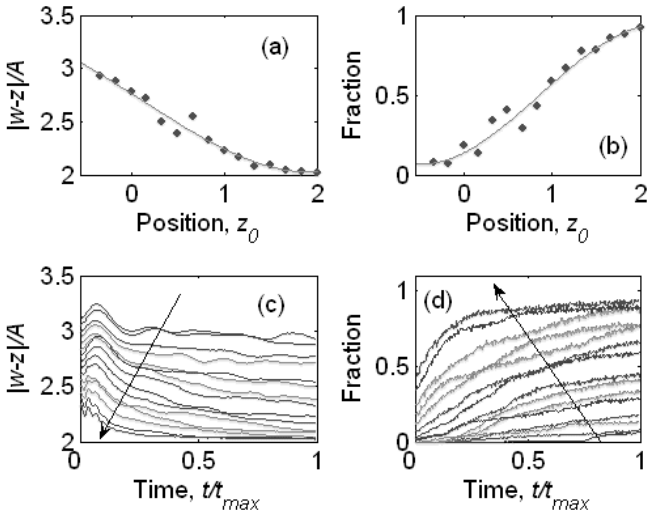

Figure 4. Mean distance (normalized to the roughness A) between the flexible tissue and the surface (a) and the fraction of the attached bonds (b) as a function of the distance z_0 at which the tissue is kept by an external force. The subplots (c) and (d), respectively, illustrate the numerical procedure described in the caption to figure 3.

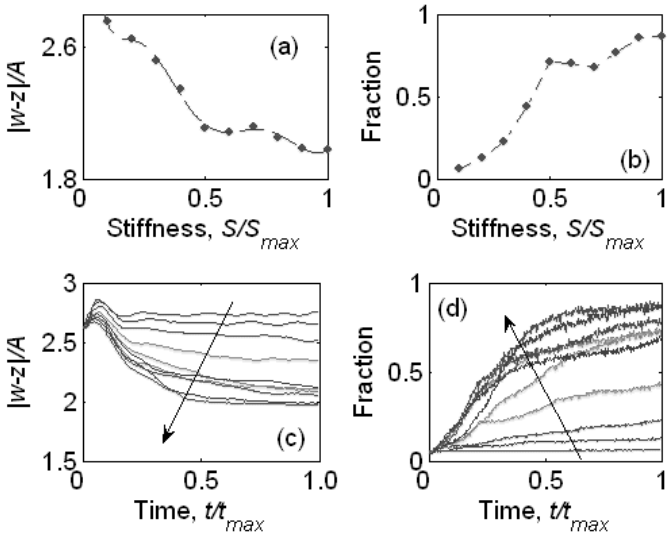

Figure 5. Mean distance (normalized to the roughness A) between the flexible tissue and the surface (a) and the fraction of the attached bonds (b) as a function of fibre stiffness. The subplots (c) and (d), respectively, illustrate the numerical procedure described in the caption to figure 3.

from a trial state with completely disconnected bonds and tends to a dynamic equilibrium. We average desirable variables over an ensemble of the fibres and calculate time dependences of the mean values. Then we omit an initial transient period and average them over the second half of the time run.

Figure 3 presents the mean distortion of the fibres (a) and the fraction of the attached bonds (b) as a function of the surface roughness. The mean distortion is defined as a transverse shift

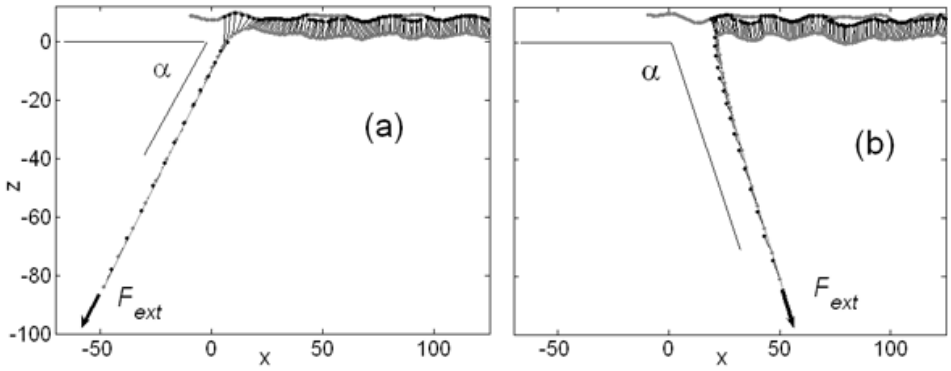

Figure 6. Instant configurations of the tissue with partially attached and detached fibres when one of the ends is pulled at an angle of $\alpha < \pi/2$ and $\alpha > \pi/2$ ((a) and (b) respectively). It is seen that the fibre configuration near surface in an instant detachment region hardly depends on the angle.

of the fibre end Δx_k normalized to the initial unperturbed length of the fibre $\sum_{j=1}^{j=n_{\max}} z_j(t=0)$ and averaged over an ensemble of fibres: $\langle \Delta x_k / \sum_{j=1}^{j=n_{\max}} z_j(t=0) \rangle$. Figure 4 shows the mean distance (normalized to the roughness A) between the flexible tissue and surface (a) and the fraction of the attached bonds (b) as a function of the distance z_0 at which the tissue is kept by an external force. The mean distance between the flexible tissue and the surface (a) and the fraction of the attached bonds (b) as a function of fibre stiffness are depicted in figure 5.

In all cases the subplots (c) and (d), respectively, illustrate the numerical procedure. A family of curves in each subplot presents time dependences of the respective variable for different parameter values. An increase in the parameter is shown by the arrow. Time intervals of the transient process and asymptotic dynamic equilibrium are seen directly from the time dependences of the variables.

In fact, the main result of the simulations is summarized in the combination of figures 3(a) and (b). It is seen directly that when the surface roughness A increases it provokes a stronger distortion of the fibres. *This distortion compensates for the roughness almost completely up to a few orders of amplitude of A*. In other words, while the amplitude is changed in a wide interval the fibres are able to keep almost perfect contact between the surfaces due to their transverse motions.

In its turn, alternating distortions of the fibres in different directions should change the scenario of detachment of the system from the surface when it is pulled by an external force. In particular, one can expect weak dependence of the detachment process on the pulling angle α [14] in a wide region of the angles around normal pulling $\frac{\pi}{2} - \delta\alpha < \alpha < \frac{\pi}{2} + \delta\alpha$. To check this hypothesis, we performed a simulation of the pulling in the geometries presented in figures 6(a) and (b) for both $\alpha < \frac{\pi}{2}$ and $\alpha > \frac{\pi}{2}$, respectively. The figures present typical instant configurations appearing in the numerical experiment. As can be seen from the pictures, the local detachment process strongly depends on a particular orientation of the fibres in the vicinity of the detaching end then on the direction of the external force F_{ext}.

Figures 7(a) and (b) present the results of the simulations. The numerical procedures here differ slightly from the previous ones because pulled tissue cannot attain a dynamic equilibrium. The procedures are illustrated in subplots (c) and (d), respectively. First we allow the system to get an attached state into dynamic equilibrium and pull after one of the ends. The process is continued up to a fixed time moment t_{final} (which is fixed to be the same for all the angles α). We record the distance of the pulled end from the surface and the fraction of fibres which

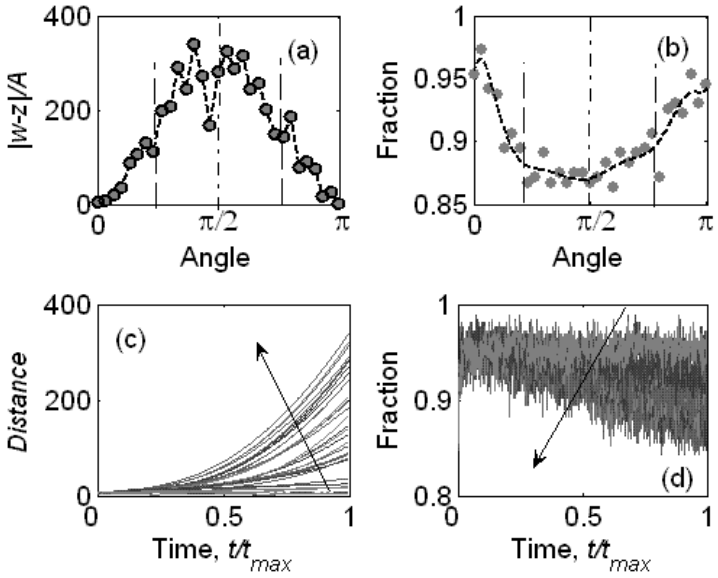

Figure 7. Angle dependences of the instant distance of the pulled end (a) and the fraction of attached bonds (b) obtained for the process shown in figure 6. The numerical procedures for the calculations are illustrated in (c) and (d), respectively. First we allow the system to get an attached state (in dynamic equilibrium) and pull one of the ends up to a fixed time moment (the same for all the angles). The resulting distance and fraction here are taken at the final time moment and averaged over the ensemble only.

remain attached at $t = t_{\text{final}}$. The longer the distance achieved (the fewer fibres remaining attached) the more effective is the pulling process. It is seen from the subplots (a) and (b) that the detachment hardly depends on α over a wide interval of angles $\frac{\pi}{4} \leqslant \alpha \leqslant \frac{3\pi}{4}$.

3. Conclusion

An artificial structure of a flexible tissue with elastic fibres that contact with a rough fractal surface by van der Waals forces is studied numerically. To study this problem an advanced model has been constructed. It includes: flexible soft tissue, relatively hard fibres attached to the tissue, an adhesive surface that attracts the ends of the fibres by the van der Waals potential and has a fractal structure with a given Fourier spectrum and amplitude of roughness. The random noise and external pulling force simulating an interaction of the system with the environment are also incorporated into the model. A set of numerical simulations has been performed with the model in the following standard procedure. A flexible tissue was placed at some initial distance z_0 from a numerically generated fragment of random rough surface and was allowed to self-organize naturally according to the model equations.

The results favour the conclusion that transverse motion leads to a strong redistribution of the fibres along the surface. It compensates for fractal surface structure in the z-direction. As a result, the tissue is efficiently attracted by the fibres to the surface and finally matches it with an extremely large contact area for a wide variation of surface roughness A. Similarly, transverse distortions of the fibres strongly affect the scenario of their detachment from the surface when the tissue is pulled off by an external force. The detachment process at every local point depends on a random orientation of the fibres caused by surface randomness and hardly depends on the direction of the external force F_{ext} for a wide interval of pulling angles α.

Acknowledgments

One of the authors (AF) is grateful to the European Science Foundation and Deutsche Forschungsgemeinschaft for financial support during his stays at Berlin Technological University: grants 956 Nanotribology (NATRIBO) and 436 UKR 17/9/06.

References

[1] Autumn K *et al* 2000 *Nature* **405** 681–5
[2] Autumn K *et al* 2002 *Proc. Natl Acad. Sci. USA* **99** 12252–6
[3] Cappella B and Dietler G 1999 *Surf. Sci. Rep.* **34** 1–104
[4] Persson B N J 2003 *J. Chem. Phys.* **118** 7614–21
[5] Persson B N J, Albohr O, Tartaglino U, Volokitin A I and Tosatti E 2005 *J. Phys.: Condens. Matter* **17** R1–62
[6] Scherge M and Gorb S 2001 *Biological Micro- and Nano-Tribology* (Berlin: Springer)
[7] Sitti M and Fearing R S 2003 *J. Adhes. Sci. Technol.* **17** 1055–957
[8] Geim A K, Dubonos S V, Grigorieva I V, Novoselov K S, Zhukov A A and Shapoval S Yu 2003 *Nature* **2** 461–3
[9] Northen M T and Turner K L 2005 *Nanotechnology* **16** 1159–66
[10] Yurdumakan B, Raravikar N R, Ajayan P M and Dhinojwala A 2005 *Chem. Commun.* 3799–801
[11] Persson B N J and Gorb S 2003 *J. Chem. Phys.* **119** 11437–44
[12] Campolo D, Jones S D and Fearing R S 2003 *IEEE Nano 2003 (San Francisco, Aug. 2003)*
[13] Majidi C *et al* 2006 *Phys. Rev. Lett.* **97** 076103
[14] Autumn K *et al* 2006 *J. Exp. Biol.* **209** 3569–79
[15] Filippov A E and Popov V 2006 *Phys. Lett.* A **358** 309–12

Queries for IOP paper 235571

Journal: **JPhysCM**
Author: **A E Filippov and V Popov**
Short title: **Flexible tissue with fibres interacting with an adhesive surface**

Page 10

Query 1:-
Author: [7]: Please check the page range.
